

Direct-conversion flat-panel X-ray image detectors

S.O. Kasap and J.A. Rowlands

Abstract: Flat-panel X-ray image detectors have been shown to be suitable to replace the conventional X-ray film/screen cassettes for medical radiography (static or snapshot imaging). They are capable of capturing the X-ray image digitally immediately after the X-ray exposure which permits a convenient clinical transition to digital radiography. There are two general approaches to the flat-panel X-ray detector technology: direct and indirect conversions. The authors review the operating principles for direct conversion, and formulate and review the required X-ray photoconductor properties for enabling a successful direct conversion detector. Two important photoconductor requirements are discussed in detail, the X-ray sensitivity and dark current, both of which are topical current research areas in seeking the best photoconductor amongst a number of candidate semiconductors such as a-Se, PbI_2 , HgI_2 and others. The requirements of medical fluoroscopy (real-time imaging at very low exposure levels) is challenging this technology and demanding even higher X-ray sensitivity.

1 Introduction to digital X-ray imaging

An ideal X-ray system would permit the instantaneous acquisition of an X-ray image in digital form with the use of the theoretical minimum number of X-rays. Partial steps towards this goal have been achieved using transitional approaches. However, now it is possible using flat-panel detectors to approach the ideal system.

Conventionally, snapshot images or radiographs are obtained using a film in close contact with a light-emitting phosphor layer or screen. X-rays impinging on the screen give off light that exposes the film creating a latent image that is subsequently amplified and made permanent by the chemical development process. This is the film/screen system where the film and screen are coupled in a portable cassette.

Medical X-ray imaging has recently made advances, such as improved films and screens, reduced exposure rates and improved equipment, but still 65% of X-ray imaging is accomplished with film/screen systems. The cassettes are loaded with film and taken to the examination room, then to the X-ray equipment and after exposure they are returned to the darkroom for development before a final image can be viewed. This is time consuming and an ideal digital system could eliminate this process.

The transitional digital systems used to achieve aspects of the ideal digital system have been based on the use of photostimulable phosphor plates, X-ray image intensifiers coupled to optical charge coupled devices (CCD) arrays and phosphor screens directly coupled optically to CCDs [1]. With photostimulable plate systems the X-ray image is captured on a photostimulable plate, which must then be

taken to and scanned by a laser system to digitise the image information. This is just as time consuming as for conventional film/screen systems and furthermore the image quality is not as good. With X-ray image intensifier systems the image is obtained instantaneously but the image quality for radiography is also poorer than for film/screen and the X-ray image intensifier is bulky and extremely expensive which limits its use to situations where the real time aspects of the image are also important. The basis of optically coupled CCD systems involves the use of a structured screen (such as Tl activated CsI phosphor), which is able to collect X-rays and convert them to light, which is then collected by tapered optical fibres. This reduces the image size by a factor of 2–4 and matches the size of the CCD array, typically no larger than 2×2 cm to the required field of view of the clinical task. For fields of view larger than 10×10 cm several CCDs must be used together to obtain a detector of sufficient size for many clinical studies.

There is still a need for an ideal digital X-ray imaging system. What would such a system provide? It should first provide a reduction in X-ray exposure or dose. The image should be of a high quality and be available almost immediately such that it would be available for use in real-time imaging (e.g. digital cine loops and fluoroscopy). It would be so designed as to minimise cost and thus conveniently incorporated into medical systems. The ideal system would record the X-ray image directly onto a computer where it could be read, stored and analysed. Such a system can be achieved using a flat-panel X-ray image detector as illustrated in Fig. 1 for mammography.

Research over the past ten years [2] has indicated that the most practical flat-panel system would be based on a large-area integrated circuit. Such large integrated circuits or active matrix arrays have been developed as the basis for large-area displays. Active matrix arrays (AMA) based on hydrogenated amorphous silicon (a-Si:H) thin-film transistors (TFTs) have been shown to be practical image addressing systems. They may be converted into X-ray sensitive imaging devices by adding a thick (~ 1 mm) X-ray detecting medium. Systems using either a phosphor or a photoconductor are possible. The active matrix array used for image addressing and readout in a flat-panel X-ray

© IEE, 2002

IEE Proceedings online no. 20020350

DOI: 10.1049/ip-cds:20020350

Paper first received 19th April and in revised form 25th October 2001

S.O. Kasap is with the Department of Electrical Engineering, University of Saskatchewan, Saskatoon, Canada S7N 5A9

J.A. Rowlands is with the Departments of Medical Imaging and Medical Biophysics, University of Toronto, Sunnybrook and Women's College Health Science Centre, 2075 Bayview Avenue, Toronto, Canada M4N 3N5

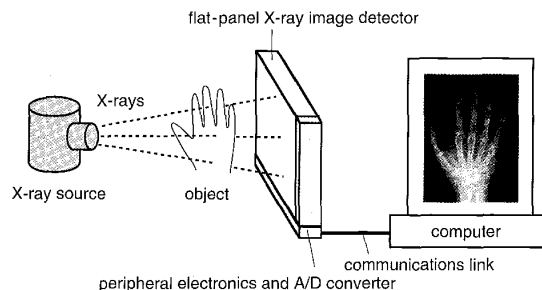


Fig. 1 Flat panel X-ray image detector

Connection from the detector to a local or distant computer is a convenient communications link e.g. wireless link allowing a more versatile detector usage

image detector consists of many single pixels, each of which represents a corresponding pixel of the image. Each pixel has some charge that is proportional to the X-ray radiation that it receives. To generate this signal charge, either a phosphor is used to convert the X-rays to visible light which in turn is detected with a p-i-n photodiode at the pixel (indirect) or an X-ray photoconductor converts the incident X-rays to charge (direct) in one step. Several manufacturers and academic researchers have used the indirect approach. However, the present authors believe that the direct

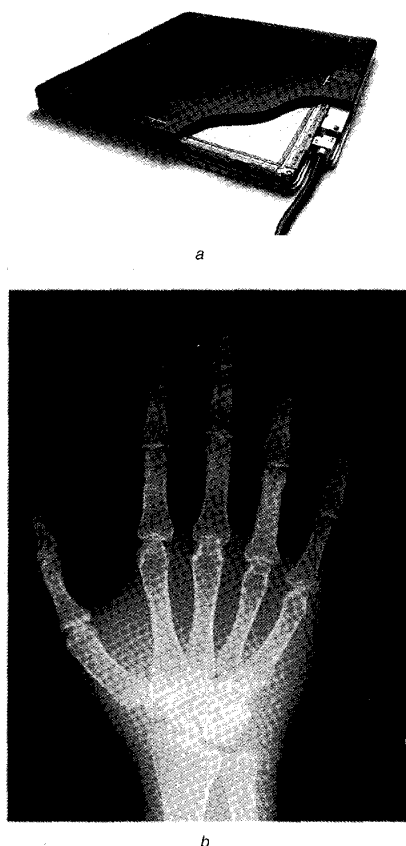


Fig. 2 Flat panel active-matrix direct-conversion X-ray image sensor using stabilised α -Se as photoconductor (Courtesy of Direct Radiography Corp.)

a Photograph of sensor. Sensor is 14 in \times 17 in; active matrix array size 2480×3072 ; pixel size $139 \mu\text{m} \times 139 \mu\text{m}$; 7.9 million pixels
b Scaled X-ray image of a hand obtained using sensor in *a*

approach should produce systems that are superior in image quality to indirect conversion sensors and are also easier and cheaper to manufacture owing to their simpler structure. This review discusses the principles involved in such direct imaging systems and the advantages and limitations in the areas of sensitivity, noise and dark current for photoconductors. Fig. 2 shows a photograph of a direct conversion flat-panel X-ray image detector.

2 Direct conversion X-ray image detector principles

2.1 Active matrix readout

Active matrix arrays allow monolithic imaging system of large areas (e.g. $40 \times 40 \text{ cm}$) to be constructed. As for conventional integrated circuits, planar processing of the array through deposition and doping of lithographically masked individual layers of metals, insulators and semiconductors implement the design of active matrix arrays. In the future, even larger areas should become feasible if required. Millions of individual pixel electrodes in the matrix and are connected, as in Fig. 3. Each pixel has its own thin-film transistor (TFT) switch allowing electrodes passing over the array to obtain charges, which are taken to subsidiary electronics on the periphery. The TFT switches control the image charge so that one line of pixels is activated electronically at a time. Normally all the TFTs are off, permitting the latent image charge to accumulate on the array. The readout is achieved by external electronics and software controlling the state of the TFT switches. The active matrix array consists of $M \times N$ (e.g. 2480×3072) storage capacitor C_{ij} whose charge can be read through properly addressing the TFT (i, j) via the gate i and source j lines. The charges read on each C_{ij} are converted to a digital image as subsequently described. The readout is essentially self-scanning in that no external means such as a laser is used. The scanning is integral to the flat-panel detector and its electronics and software.

The self-scanned readout of the active matrix involves the coordinated operation of the TFTs, which is facilitated by

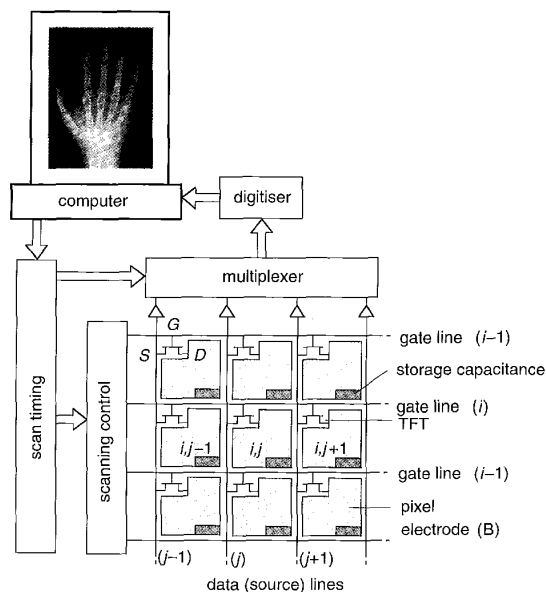


Fig. 3 Thin-film transistor active matrix array for use in X-ray image detectors with self-scanned electronic readout

Charge distribution residing on panel's pixels are simply read out by scanning the arrays row-by-row using peripheral electronics and multiplexing parallel columns to a serial digital signal

the structure of the array. The gates of all the TFTs in each row are connected to the same gate control line. The TFTs in each column are connected by their source to a common readout or data line. If gate i is activated, it means the TFTs in that particular row are 'on' and N data lines (from $j = 1$ to N) will read the charges on the pixel electrodes in row i . From this beginning the parallel data are multiplexed, serialised and digitised to the computer for imaging. Then the next row $i + 1$ is activated by the scanning control and the process is repeated until all rows have been activated and processed.

2.2 X-ray photoconductor and AMA integration

To construct a direct-conversion flat-panel X-ray imager the active matrix array is coated with an X-ray photoconductor, shown in Fig. 4, which in this example consists of stabilised a-Se. To permit the application of an electrical field F , a metal electrode A is deposited onto the a-Se layer. This electrode may have either a positive or negative applied bias voltage. In one type of sensor that operates with a positive bias, there is a thin dielectric (insulating) layer between the a-Se and the top electrode A. A second layer, doped a-Se alloy, is coated between the pixel charge collection electrode B and a-Se to reduce the injection of electrons, and hence the dark current, from the metal B into the photoconductor, discussed as follows.

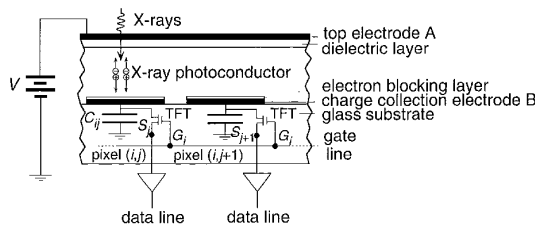


Fig. 4 Simplified schematic diagram of cross-sectional structure of two pixels of a-Se self-scanned X-ray image detector

Electron-hole pairs generated in the photoconductor by the absorption of an X-ray photon must travel along the field lines and are collected by the pixel electrodes and stored on the pixel capacitors to form a latent charge image. If the applied bias voltage is negative, holes collect at the negative bias electrode and electrons on the storage capacitor C_{ij} . Thus after the X-ray exposure of the object to be imaged a latent image consisting of an amount of charge ΔQ_{ij} proportional to the amount of incident X-ray radiation is carried by each pixel capacitor C_{ij} , i.e. the charge is proportional to the X-rays absorbed in the pixel's photoconductor directly above it. To readout the latent image charge ΔQ_{ij} the appropriate TFT is turned on every Δt seconds and the charge is transferred to the data line and hence to the charge amplifier on the periphery of the array.

For a-Se based photoconductors the applied bias is several kilovolts. The capacitance C_{pc} of the a-Se layer over the pixel is much smaller than the pixel capacitance so that the majority of the applied voltage drops across the photoconductor. If the panel is left without scanning, dark current or signal current from X-ray irradiation will cause the potential on the pixel electrode to rise towards the applied bias voltage. A voltage of ~ 50 V across the TFT can result in breakdown and permanent damage to the TFT. There are various methods for protecting the TFT from damage. The simplest method is to use a negative bias on A; voltage in Fig. 4 is reversed. As negative potential voltage collects in the pixel electrode, eventually sufficient

charge accumulates that the TFT is partially turned on (gate voltage is not negative enough to turn off the TFT) thus preventing a damaging potential from accumulating on the pixel. In the case of positive bias (Fig. 4), under excessive exposure the trapped electrons at the dielectric/a-Se interface collapse the field in the photoconductor as indicated in Fig. 5. However, this protection results in increased read out complexity which must eliminate the trapped charges at the a-Se/dielectric layer before subsequent exposures. This is achieved by removal of the applied bias voltage and flooding the detector with light to photogenerate carriers in a-Se that flow in the opposite direction to that generated by the X-rays. The requirement of a refresh cycle makes this approach to high-voltage damage protection incompatible with fluoroscopic (i.e. real-time read-out) applications.

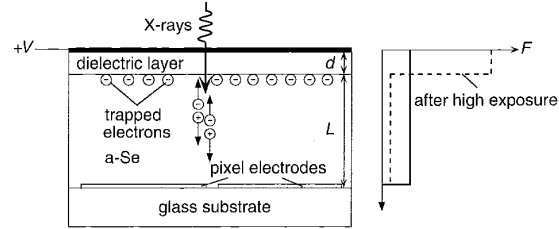


Fig. 5 Trapped electrons at interface between dielectric layer and photoconductor collapse field in photoconductor so that no further charge can accumulate on pixel electrodes; thus TFT is prevented from breakdown under high exposure

Fig. 6a shows the conventional equivalent circuit of the pixel detector described, where V is the applied voltage, V_{pc} is the bias voltage across the photoconductor, C_{px} is the pixel storage capacitor (C_{ij} in Fig. 4), C_{pc} is the capacitance of the photoconductive layer, V_{px} is the voltage on the pixel storage capacitor, and I_{ph} is the X-ray photocurrent. The dark current is taken as negligibly small, which is not always the case as discussed subsequently. Since $C_{pc} \ll C_{px}$, V_{pc} is almost the same as the applied voltage V . It is possible to protect the TFT by other methods and also maintain the real-time capability such as by inserting a Zener-diode voltage protection at the pixel electrode as in Fig. 6b or by using a dual gate TFT as in Fig. 6c. The bias voltage V_{bias} in Fig. 6b allows the maximum pixel voltage to be controlled. The second gate (top gate TG in the Fig. 6c) on the TFT turns the transistor on when the potential V_{px} rises beyond a safe level controlled by the top-gate dielectric layer thickness. Because the excess charge is bled away along the read-out lines, there is the potential for corruption of image information of pixels sharing the same read out line with overexposed pixels.

3 X-ray photoconductor design

The performance of direct-conversion X-ray sensors depends critically on the selection and design of the photoconductor. It is therefore instructive to identify what constitutes a nearly ideal X-ray photoconductor to motivate a search for improved performance or better materials. Ideally, the photoconductive layer should possess the following material properties:

- Most of the incident X-ray radiation should be absorbed within a practical photoconductor thickness to avoid unnecessary patient exposure. This means that over the energy range of interest, the absorption depth δ of the X-rays must be substantially less than the device layer thickness L .

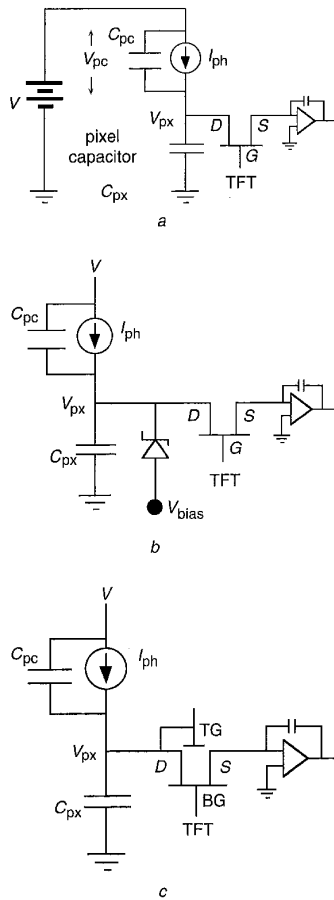


Fig. 6 IFT protection
a Conventional circuit
b Zener diode circuit
c Dual-gate TFT

- The photoconductor should have high intrinsic X-ray sensitivity, i.e. it must be able to generate as many collectable (free) electron-hole pairs (EHPs) as possible per unit of incident radiation. This means the amount of radiation energy required, denoted as W_{\pm} , to create a single free electron and hole pair must be low because the free (or collectable) charge ΔQ generated from an incident and absorbed radiation of energy ΔE is simply $e\Delta E/W_{\pm}$. Typically W_{\pm} increases with the bandgap E_g of the photoconductor.

- There should be no bulk recombination of electrons and holes as they drift to the collection electrodes; EHPs are generated in the bulk of the photoconductor. Bulk recombination is proportional to both the concentration of holes and electrons and typically it is negligible provided the instantaneous X-ray exposure is not too high.

- There should be negligible deep trapping of EHPs which means that, for both electrons and holes, the schubweg $\mu\tau F \gg L$ where μ is the drift mobility, τ is the deep trapping time (lifetime), F is the electric field and L is the layer thickness. The schubweg is the distance a carrier drifts before it is trapped and unavailable for conduction.

- The dark current should be negligibly small. This means the contacts to the photoconductor should be non-injecting and the rate of thermal generation of carriers from various defects or states in the bandgap should be negligibly small (i.e. dark conductivity is practically zero). Small dark

conductivity generally requires a wide bandgap semiconductor which conflicts with the second condition.

- The longest carrier transit time, which depends on the smallest drift mobility, must be shorter than the access time of the pixel and interframe time in fluoroscopy.

- All this should not change or deteriorate with time and as a consequence of repeated exposure to X-rays, i.e. X-ray fatigue and X-ray damage should be negligible.

- The photoconductor should be easily coated onto the AMA panel, for example, by conventional vacuum techniques without raising the temperature of the AMA to damaging levels (e.g. $\sim 300^{\circ}\text{C}$ for a-Si panels). Special processes are generally more expensive. The photoconductor should be coatable on a large area substrate. A large-area detector is essential in radiography since the lack of a practical means to focus X-rays necessitates a shadow X-ray image, which is larger than the body part to be imaged.

The large-area coating requirement over areas typically $30 \times 30 \text{ cm}$ or greater rules out the use of X-ray sensitive crystalline semiconductors which are difficult to grow in such large areas. Thus, the only practical way in which crystalline materials can be used is to crystallise them separately and then connect them with indium bump bonds to the substrate, a process that is very expensive which limits its application to small area devices. Although various polycrystalline X-ray photoconductor materials are currently in commercial use, most of their device applications still also involve small areas, typically less than 10 cm^2 e.g. CdTe, CdZnTe, CdSe, PbO, Pbl₂, Hgl₂. For example, both CdSe and PbO are used in polycrystalline form in one-inch diameter X-ray vidicons available commercially. Recent experiments on larger area Pbl₂ and Hgl₂ polycrystalline X-ray photoconductive layers on active matrix array have shown encouraging results [3, 4]. However, due to its commercial use as an electrophotographic photoreceptor, a-Se is one of the most highly developed photoconductors [5, 6]. It can be easily coated as thick films (e.g. $100\text{--}1000 \mu\text{m}$) onto suitable substrates by conventional vacuum deposition techniques and without the need to raise the substrate temperature beyond $60\text{--}70^{\circ}\text{C}$. Its amorphous state maintains uniform characteristics to very fine scales over large areas. Thus currently a-Se is still the only practical photoconductor for clinical medical X-ray sensors because it has an acceptable X-ray absorption coefficient, good charge transport properties for both holes and electrons and the dark current in a-Se is much smaller than many competing polycrystalline layers [7].

4 X-ray sensitivity

The X-ray sensitivity of a direct-conversion imaging sensor depends on the X-ray sensitivity of the photoconductor that converts the absorbed radiation to charge collected. The sensitivity is usually addressed in terms of three controlling factors. The first factor is how much radiation is actually absorbed from the incident radiation that is useful in the photoelectric effect. The second is the generation of EHPs, i.e. a quantity of charge ΔQ , from the absorbed radiation. The third factor is how much of the photogenerated charge ΔQ is actually collected in the external circuit. The first factor is characterised by the quantum efficiency, the second by the EHP creation energy and the third factor by the charge carrier drift mobilities and lifetimes.

4.1 X-ray quantum efficiency

It is highly desirable in medical imaging for the photoconductor to absorb as much of the incident radiation

energy as possible to minimise patient exposure. The fraction $A_Q(E)$ of incident photons with energy E in the beam that are attenuated by the photoconductor depends on the linear attenuation coefficient α of the photoconductor material and its thickness L and is given by

$$A_Q(E) = \text{attenuated fraction} = [1 - \exp(-\alpha L)] \quad (1)$$

where $\alpha = \alpha(E, Z, d)$ is the linear attenuation coefficient of the material and is a function of energy E , atomic number Z and density d of the material. A_Q is called the 'quantum efficiency' because it describes the efficiency with which the medium attenuates photons. The reciprocal of α , $1/\alpha$, is the attenuation depth δ where the beam has been attenuated by 63%. If each photon has an energy E , the actual energy absorbed per photon, neglecting secondary photon absorption, is given by $E(\alpha_{en}/\alpha)$ where α_{en} is the energy absorption coefficient that depends on E , Z and d . The actual energy deposited into the photoconductor is then given by

$$E_{\text{absorbed}} = \int_0^{E_{\text{max}}} \Phi(E) E \frac{\alpha_{en}(E)}{\alpha(E)} (1 - \exp[-\alpha(E)L]) dE \quad (2)$$

where $\Phi(E)$ is the photon fluence per unit energy, i.e. number of photons arriving per unit area per unit energy, which is the energy spectrum of the X-ray beam. The energy absorbed by a given photoconductor material can be maximised by making the detector thickness L several times the attenuation depth δ . Table 1 summarizes the attenuation depth for a selection of potential X-ray photoconductors at photon energies 20 and 60 keV, corresponding very approximately to mean energies used in mammography and chest radiology.

The minimisation of dosage requires the absorption depth such that the most of the radiation is absorbed within the thickness L , or $\delta < L$. The required photoconductor thickness has to be several times the absorption depth δ ; this means that it depends on the photon energy hence the particular imaging application and the locations of the K and L-edges. The K-edge of a-Se is ~ 12.7 keV making it particularly useful for mammographic applications. For mammography with mean photon energy of 20 keV, the required a-Se thickness, taken as 2δ , is about 100 μm ; for chest radiology it is about 2000 μm with mean photon energy of 60 keV. For comparison, the corresponding thicknesses for an HgI_2 detector are about 60 μm and 500 μm , respectively.

Although increasing the detector thickness L increases the fraction of absorbed photons, there are three main factors that limit L : First, as L is increased, there is a higher probability the X-ray generated charges will be trapped as they drift across greater distances to reach the electrodes, i.e. the sensitivity may become schubweg-limited as discussed

subsequently. Secondly, a practical means by which cost-efficient, thick photoconductor layers can be fabricated without defects. Thirdly, the overall applied voltage for a given electric field is proportional to L .

4.2 Ionisation energy W_{\pm}

The amount of radiation energy W_{\pm} absorbed by a medium to create a single free electron-hole pair (EHP) is called the ionisation energy or the EHP creation energy. This must be as low as possible because the free (or collectable) charge ΔQ generated from an absorbed radiation of energy ΔE is simply $e\Delta E/W_{\pm}$.

The creation of EHPs by an incident energetic particle or an X-ray photon first involves the generation of an energetic primary electron from an inner core shell, for example, the K-shell. As this energetic photoelectron travels in the solid, it causes ionisation along its track and hence the creation of many EHPs. For many semiconductors the energy W_{\pm} required to create an EHP has been shown to depend on the energy bandgap E_g by Klein's rule

$$W_{\pm} \simeq 2.8E_g + E_{\text{phonon}} \quad (3)$$

The phonon energy term E_{phonon} is small (< 0.5 eV) so that typically W_{\pm} is close to $2.8E_g$. Further, in many crystalline semiconductors W_{\pm} is field independent and well defined. This W_{\pm} is so well defined in crystalline semiconductors, such as high purity Si and Ge crystals that they are used in spectrometers to measure the energy of X-rays [8]. Table 1 summarises the EHP creation energy W_{\pm} and the bandgap energy E_g for a variety of semiconductors. The photoconductor requirement of negligible dark currents implies that the semiconductor should have a wide bandgap which, however, leads to a higher W_{\pm} and lower X-ray sensitivity. The W_{\pm} expression in (3) normally excludes the loss of charges that arise from the recombination and trapping of photogenerated electrons and holes as they drift to the collecting electrodes. When such effects are included, the observed W_{\pm} would be an effective ionisation or EHP creation energy and would obviously be greater than that in (3).

There are also various solids such as stabilised a-Se that exhibit a field-dependent W_{\pm} whose origin has not been conclusively identified and is currently a topical research area [7]. In the case of a-Se, W_{\pm} at a given X-ray energy E decreases with the electric field F approximately as

$$W_{\pm} \simeq W_{\pm}^0 + \frac{B}{F} \quad (4)$$

where B is a constant that depends on the energy and W_{\pm}^0 is the saturated EHP creation energy (at infinite field). W_{\pm} also has a weak photon energy dependence but this is neglected in (4). Table 1 lists W_{\pm} for a-Se at the field of 10

Table 1: Densities, attenuation depths ($\delta = 1/\alpha$) at photon energy of 20 and 60 keV and energy bandgaps (E_g) of selected potential X-ray photoconductor materials

Photoconductor	TlBr	PbO	PbI ₂	HgI ₂	Ge	GaAs	a-Se	GaSe	ZnTe	CdS	CdSe	CdTe
Density (g cm ⁻³)	7.5	9.8	6.1	6.3	5.32	5.31	4.3	4.6	6.34	4.82	5.81	6.06
δ (μm) at 20 keV	18	11.8	28	32	44	44	48	49	58	127	56	77
δ (μm) at 60 keV	317	218	259	252	929	926	976	1026	300	439	385	250
E_g (eV)	2.7	1.9	2.3	2.1	0.7	1.42	2.3	2.0	2.26	2.3	1.8	1.5
W_{\pm} (eV)	6.5	8-20	5	4-7	1.5	6.3	45*, 20†	6.3	7	7.2	5	4.65

*at $F = 10 \text{ V}/\mu\text{m}$

†at $F = 30 \text{ V}/\mu\text{m}$

X-ray mass attenuation coefficients data from <http://physics.nist.gov/PhysRefData/XrayMassCoef/cover.html>

V/ μm and 30 V/ μm . In the past the typical value of the electric field used in a-Se devices was ~ 10 V/ μm where the value of W_{\pm} is 40–50 eV. Direct metal to a-Se contacts used in the early work limited the maximum field strength to ~ 10 V/ μm . The recent development of improved blocking layers permits the electric field to be increased beyond this value [9] and at the same time keep the dark current at a low value. A significant increase in signal should therefore be possible in future devices utilising these new blocking contacts. A field of 30 to 80 V/ μm is high enough to increase the signal, but low enough to avoid the potential complications of the avalanche region (i.e. absorption depth dependent gain). The current theoretical and experimental interest in characterising and understanding the EHP creation energy in amorphous semiconductors is expected to continue, given the importance of this class of materials in large area X-ray photoconductor applications.

Recently there has been active research to find potential candidate X-ray photoconductors to replace a-Se in flat-panel sensors. The reason is that despite its various distinctly favourable qualities, a-Se has three identifiable problems: (i) the very high voltage needed to operate the a-Se layer could, under fault conditions, possibly damage the a-Se active-matrix array; (ii) the lower than ideal W_{\pm} ; and (iii) the relatively low Z resulting in the requirements for very thick layers to maintain high QE.

Single-crystal PbI_2 was first investigated for nuclear radiation detectors. More recently, thin layers have been deposited onto active-matrix arrays to form an X-ray imaging system [3]. It shows an adequate schubweg provided that relatively high biasing fields (1 V/ μm) are used. PbO has also been used as an imaging photoconductor for some time. The first application (in 1954) was in an optical vidicon [10] and a large-area X-ray vidicon was made in 1956 [11]. The vidicon tube was 8 inches in diameter and had a 150 μm -thick layer of PbO in a p-i-n structure. The p and n-regions were obtained by doping the PbO ; the intrinsic region was obtained by making the PbO porous. A value of W_{\pm} that is ~ 8 eV has been reported for crystalline PbO but higher values for evaporated layers [12]. It is difficult to manufacture PbO layers because PbO reacts immediately with ambient air, causing both its dark resistance and its X-ray sensitivity to decrease. A more serious problem with thick layers is the degradation with use characterised by image persistence, nonuniformity, white spots, and decreasing sensitivity [13]. It has also been used for the construction of prototype flat-panel imaging systems [12]. TlBr [14] is a crystalline semiconductor with a high ionic conductivity that gives rise to a large dark current. However, sufficiently good films have been made that it has been used as the photoconductor for large-area vidicons where it is cooled with a Peltier cooler [15] to reduce the ionic current to negligible levels. There is a host of other materials under investigation as potential photoconductors for medical X-ray imaging including CdTe [16], CdZnTe , and HgI_2 [17, 18]. Indeed, recent research on HgI_2 layers has shown that this photoconductor can be deposited to exhibit both low dark currents and acceptable charge carrier schubwegs at reasonable applied fields. Good images have been demonstrated using HgI_2 as a photoconductor on an AMA. In the coming years it is likely that many of these will be combined with active-matrix arrays to investigate their potential for diagnostic radiology. New engineered materials known as nanocomposite organic photoconductors [19], consisting of nanoparticles of heavy metals in an organic photoconductor matrix, also hold promise.

5 Charge transport and absorption limited X-ray sensitivity

The overall X-ray sensitivity S of a photoconductor may be defined as the charge Q collected per unit area per unit incident radiation, i.e.

$$S = \frac{Q}{AX} \quad (5)$$

where X is the radiation exposure, commonly measured in Roentgens, and A is the detector area receiving the radiation. The sensitivity of an X-ray photoconductor depends on the quantum efficiency A_Q , EHP creation energy W_{\pm} , and also on the efficiency $\eta_{\text{collection}}$ of charge collection given that both electrons and holes have to be transported through the photoconductor and collected by the applied field. This collection efficiency depends on the charge carrier schubwegs $\mu\tau F$ where μ is the drift mobility and τ is the carrier lifetime and also on the recombination of X-ray generated electrons and holes. The schubweg is the distance a carrier drifts before it is trapped and thereby becomes unavailable for conduction and collection by the external circuit. The mobility μ and lifetime τ product $\mu\tau$ is called the 'carrier range'.

The absorption of photons and hence the generation of EHPs in a photoconductor occurs exponentially as indicated in Fig. 7. The collected charge from a location x in the semiconductor has to be proportioned according to the electron and hole transport using Ramo's theorem [20] and for each transport species we have to apply the Hecht [21] collection efficiency. For example for holes generated at x , the collection efficiency is

$$\eta_{\text{collection}}(\text{holes}) = \frac{\mu_h \tau_h F}{L - x} \left[1 - \exp\left(-\frac{L - x}{\mu_h \tau_h F}\right) \right] \quad (6)$$

where L is the detector thickness, μ_h and τ_h are the hole mobility and lifetime. The total collected charge can be calculated by considering the charge collected for photo-generation at x and integrating this across the detector thickness. The overall sensitivity S for a monoenergetic beam with the receiving electrode biased positively can be cast into the following normalised sensitivity s form [22]:

$$\begin{aligned} \frac{S}{S_o} = s(x_h, x_e, \Delta) &= x_h \left[\left(1 - e^{-1/\Delta} \right) + \frac{1}{\frac{\Delta}{x_h} - 1} (e^{-1/x_h} - e^{-1/\Delta}) \right] \\ &+ x_e \left[\left(1 - e^{-1/\Delta} \right) - \frac{1}{\frac{\Delta}{x_e} + 1} (1 - e^{-1/\Delta - 1/x_e}) \right] \\ &= s_{\text{hole}}(x_h, \Delta) + s_{\text{electron}}(x_e, \Delta) \end{aligned} \quad (7)$$

and

$$S_o = \left(\frac{5.45 \times 10^{13} e}{(\alpha_{\text{air}}/\rho_{\text{air}})W_{\pm}} \right) \left(\frac{\alpha_{\text{en}}}{\alpha} \right) \quad (8)$$

where α_{air} is the energy absorption coefficient of air and ρ_{air} is the density of air, α and α_{en} are the linear attenuation and energy absorption coefficients of the photoconductor material, x is the schubweg per unit thickness, $\mu\tau F/L$, Δ is the normalised attenuation depth δ/L , and the subscripts h and e on the charge transport parameters x , μ and τ refer to holes and electrons, respectively, e.g. $x_h = \mu_h \tau_h F/L$. Note that W_{\pm} is in eV, $\alpha_{\text{air}}/\rho_{\text{air}}$ is in $\text{cm}^2 \text{g}^{-1}$ so that the

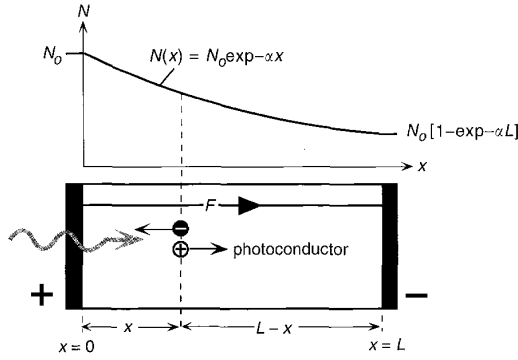


Fig. 7 Number of photons N and hence radiation energy decreases exponentially through the sample and causes electron-hole pairs to be generated in the same exponential manner

sensitivity is in $\text{C cm}^{-2} \text{R}^{-1}$. The two square brackets on the right-hand side of (7) represent the relative contributions of hole and electron transport to the overall sensitivity for a given normalised attenuation depth Δ . The right-hand side expression for the ratio S/S_0 in (7) takes into account only the charge transport and absorption effects without considering W_{\pm} .

The reason for excluding W_{\pm} in (7) is that this is a material property and can be taken as constant for a given photoconductor. For those materials that have a field dependent W_{\pm} , then S_0 depends on the field. Note that $s(x_h, x_e, \Delta) = s_{\text{hole}} + s_{\text{electron}} = 1$ when all the incident radiation is absorbed and all the charges are collected, that is $x_h, x_e \gg 1$ and $\Delta \ll 1$. The sensitivity then is simply S_0 and controlled by W_{\pm} .

Equation (7) applies to an isolated photoconductor sandwiched between two large-area parallel plate electrodes and operating under a constant field, which means that the injected charge concentration, should be small (small-signal case). There are no other electrodes other than the two parallel-plate electrodes sandwiching the sample so that small pixel effects are excluded.

The expression in (7) applies for incident radiation that is monoenergetic and has to be appropriately integrated over the radiation spectrum of the X-ray source. Furthermore, it is assumed that the radiation receiving side of the detector is biased positively. If the bias is negative the electron and hole schubwegs per unit thickness x_h and x_e have to be interchanged. Equation (7) can be used to examine the sensitivity of various photoconductor materials as a function of operating conditions (e.g. F and energy spectrum), detector thickness L or material properties and $\mu\tau$ (carrier ranges). An immediate conclusion from (7) is that the sensitivity is closely controlled by x_h and x_e as well as the normalised absorption depth Δ . The relative importance of the polarity of the carrier depends on the bias applied to the receiving electrode, the magnitudes of x_h and x_e , and the magnitude of Δ .

Fig. 8 shows the hole and electron contributions to the sensitivity s_{hole} and s_{electron} in (7), for three different values of Δ , 1/4, 1 and 4. For sufficiently long schubwegs the sensitivity contributions are nearly saturated. For example, for an a-Se mammographic detector of thickness 200 μm , for 20 keV photons, $\delta \approx 50 \mu\text{m}$ and $\Delta = 1/4$. The ratio of hole-controlled to electron-controlled sensitivity is about 3.3. Thus if the bias is positive, then the hole transport is critical; the reverse is true when the receiving electrode is negatively biased. The absence of electron transport (electrons immediately trapped) reduces the sensitivity by

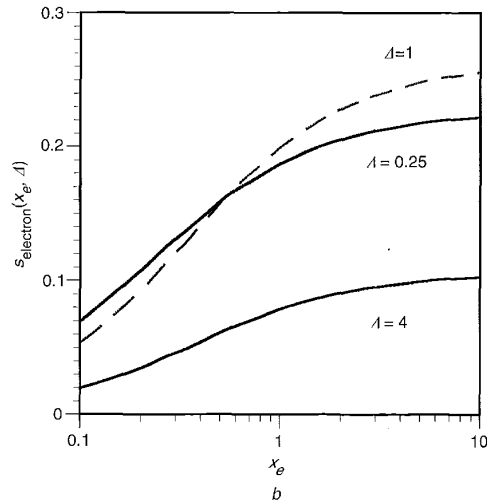
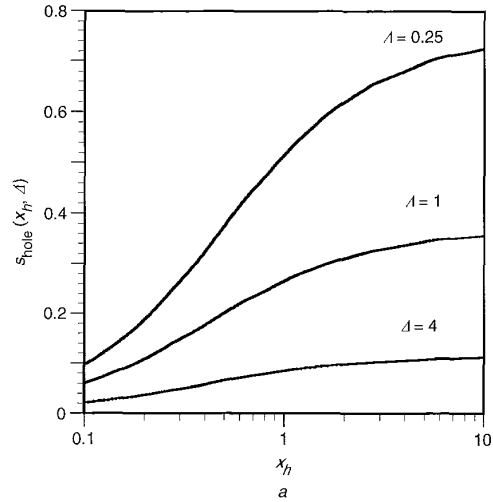


Fig. 8 Hole and electron contributions to sensitivity against x_h and x_e , respectively, for three different normalised absorption depths Δ
a $s_{\text{hole}}(x_h, \Delta)$
b $s_{\text{electron}}(x_e, \Delta)$

Total normalised sensitivity $s = s_{\text{hole}} + s_{\text{electron}}$ (unity for $x_h, x_e \gg 1$ and $\Delta \ll 1$). Positive bias on the receiving electrode

only 22% but the absence of hole transport leads to the sensitivity being cut by a factor of ~ 4.4 . The greater dependence of the X-ray sensitivity on hole trapping than electron trapping can be understood by noting that the electron and hole generation does not occur uniformly throughout the thickness of the sample but rather closer to the positive bias electrode. For 'thick' detectors $L \gg \delta$, the mean carrier generation distance is just the absorption distance δ , which is close to the positive receiving electrode. Consequently if ΔQ is the total charge of one polarity generated by X-rays all being absorbed at δ , from Ramo's theorem the external charge collected due to hole and electron transports are

$$\Delta Q_h = \Delta Q \frac{L - \delta}{L} \quad \text{and} \quad \Delta Q_e = \Delta Q \frac{\delta}{L}$$

which means that the ratio of the electron-trapping-limited to hole-trapping-limited sensitivity at 20 keV where

$\delta = 48 \mu\text{m}$, should be

$$\frac{\text{hole-trapping-limited } S}{\text{electron-trapping-limited } S} = \frac{\Delta Q_e}{\Delta Q_h} = \frac{\delta}{L - \delta} = \frac{48 \mu\text{m}}{200 \mu\text{m} - 48 \mu\text{m}} = 0.31$$

In the case of the mammographic a-Se detectors, both electron and hole schubwegs at an $F = 10 \text{ V}/\mu\text{m}$ operating field are much greater than the detector thickness so that the sensitivity is not limited by carrier schubwegs whether positive or negative bias is used. However, for higher energy a-Se detectors biased negatively, the detector thickness is $\sim 1000 \mu\text{m}$, and the sensitivity is critically controlled by the electron schubweg. Although we have only considered a-Se stabilised by alloying with approximately 0.3%As as this is the current a-Se material composition, other Se- alloys may also have potential as candidate X-ray photoconductors. One of the advantages of the a-Se-alloy material system is that it is possible to control the charge carrier ranges by appropriately alloying and doping a-Se [23, 24].

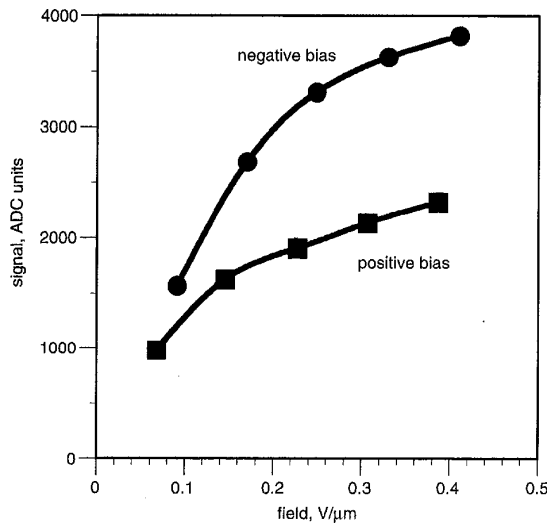


Fig. 9 Data extracted and replotted as signal against field from Fig. 8 (left) in [25]
HgI₂ 250 μm ; 100 kVp exposure

The importance of the bias polarity in relation to the relative magnitudes of the carrier ranges, as indicated in the normalised plots in Fig. 8, can be clearly seen in the HgI₂ experimental data in Fig. 9, where the relative signal against applied field has been plotted with negative and positive bias on the radiation receiving electrode. The electron range in HgI₂ is more than a factor of 10 longer than the hole range which is the reason for the observed higher sensitivity under negative bias.

Table 2 summarises various X-ray sensitivities measured on a variety of candidate photoconductors for direct conversion X-ray sensors. Although exact direct comparisons are difficult, the Table is nonetheless useful in indicating the magnitude of the signal and whether the photoconductor has any potential at all. A more rigorous comparison must include not only various noise sources but also the dark current.

6 Dark current

The dark current in an ideal photoconductor should be zero. A finite dark current accumulates charge Q_{dark} on the pixel storage capacitance $C_{\text{px}} = C_{ij}$ in Figs. 4 and 6. It is undesirable because it generates noise on the pixel and reduces the dynamic range. It is instructive to examine what constitutes an acceptable level of dark current density J_{dark} given a particular application with a specified minimum exposure and taking into account various noise sources inherent in the detection system including the quantum noise in incoming radiation. Consider a mammographic application with mean photon energy of 20 keV. The quantum noise level X_{noise} in the radiation for mammographic X-ray exposure is 60 μR . It is desirable to detect a signal that is at least as much as the quantum noise ($\text{SNR} = 1$). The charge collected due to the quantum noise in the radiation is the radiation noise signal $Q_{\text{x-noise}}$.

$$Q_{\text{x-noise}} = \frac{eAE_{1R}X_{\text{noise}}}{W_{\pm}} \quad (9)$$

where X_{noise} is in Röntgen (60 μR for mammography), E_{1R} is the energy per unit area equivalent of 1 R of radiation, A is the receiving area of the detector, W_{\pm} is the EHP creation energy and e is the elementary charge. The collected charge due to the absorption of an amount energy corresponding to the minimum likely exposure X_{min} is the minimum likely

Table 2: Sensitivity of various X-ray photoconductor candidates for flat-panel X-ray sensor applications for general radiology

Photoconductor	Reference	Sensitivity, $\text{pC mR}^{-1} \text{cm}^{-2}$	Conditions	Comment
a-Se $L = 1000 \mu\text{m}$, $F = 15 \text{ V}/\mu\text{m}$	Fig. 3 in [25]	4 400	80 kVp, 20 mm Al	Some radiation is wasted as absorption depth is comparable with L . Requires very high voltages (e.g. 10–15 kV)
HgI ₂ (polycrystalline film) $L = 150\text{--}300 \mu\text{m}$, $F \approx 0.5 \text{ V}/\mu\text{m}$	Figs. 6–9 in [4]	4 000–10 000	85 kVp + filtering	Dark current is 2–3 nA cm^{-2} with passivation
PbI ₂ (polycrystalline film) $L = 60 \mu\text{m}$, $F \approx 1 \text{ V}/\mu\text{m}$	Fig. 11 in [4]	880	80 kVp + filtering	Schubweg limited. Low field applied to keep dark current small
CdTe (polycrystalline film) $L = 200 \mu\text{m}$, $F \approx 0.1 \text{ V}/\mu\text{m}$	Fig. 4 in [16]	10 700	80 kVp + 26 mm Al	Large dark current/leakage current. Low detective quantum efficiency
CdZnTe (polycrystalline film) $L = 300 \mu\text{m}$, $F \approx 0.4 \text{ V}/\mu\text{m}$	Fig. 4a in [27]	14 000	80 kVp + 26 mm Al	Dark current 9 nA cm^{-2} at $F = 0.4 \text{ V}/\mu\text{m}$

signal Q_{signal}

$$Q_{\text{signal}} = \frac{eAE_{\text{IR}}X_{\text{min}}}{W_{\pm}} \quad (10)$$

For mammography $X_{\text{min}} = 0.6 \text{ mR}$.

The dark current I_{dark} will accumulate a quantity of charge Q_{dark} in the absence of any radiation and this constitutes the dark signal

$$Q_{\text{dark}} = AJ_{\text{dark}}\Delta t \quad (11)$$

where Δt is the time interval between pixel reading times, about 1 s for radiology (and 1/30 s for fluoroscopy). The stochastic fluctuations in the collected number of carriers on C_{px} will constitute a noise signal that is given by $Q_{\text{noise}} = e(Q_{\text{dark}}/e)^{1/2}$, i.e.

$$Q_{\text{noise}} = e\sqrt{\frac{J_{\text{dark}}A\Delta t}{e}} \quad (12)$$

The photoconductor- C_{px} -TFT switch system has thermal noise. When the TFT is on, its resistance is small and thermal fluctuations in this resistance lead to charge fluctuations on the C_{px} called kTC noise. When the TFT is turned off, a random thermal fluctuation amount of charge is left on C_{px} which constitutes noise. (In fact, thermal fluctuations in the resistance of the photoconductor would also lead to charge fluctuations but the photoconductor has a very high resistance and the time scale is very long). The kTC or thermal noise is given by

$$Q_{\text{thermal}} = \sqrt{2kTC_{\text{px}}} \quad (13)$$

where k is the Boltzmann constant and T is the absolute temperature.

Fig. 10 shows the equations plotted as $V_{\text{signal}} (= Q_{\text{signal}}/C_{\text{px}})$, $V_{\text{x-noise}} (= Q_{\text{x-noise}}/C_{\text{px}})$, $V_{\text{dark}} (= Q_{\text{dark}}/C_{\text{px}})$, V_{noise}

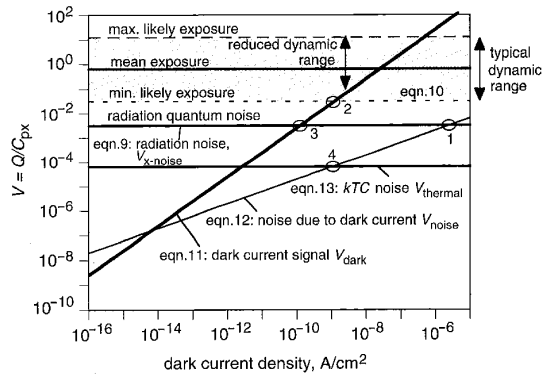


Fig. 10 Various voltages across storage capacitor C_{px} taken as 1 pF as function of dark current density given $\Delta t = 1 \text{ s}$ (radiological application)
Pixel size $50 \mu\text{m} \times 50 \mu\text{m}$; mean photon energy 20 keV; minimum and maximum radiation values 0.6 mR and 240 mR; mean radiation 12 mR; noise 60 μR

($= Q_{\text{noise}}/C_{\text{px}}$), $V_{\text{thermal}} (= Q_{\text{thermal}}/C_{\text{px}})$, i.e. as voltages developed across C_{px} , against the dark current density J_{dark} . It is assumed that as a typical value $W_{\pm} \approx 5 \text{ eV}$, and mammographic application, i.e. pixel area $A = 50 \times 50 \mu\text{m}$, and $\Delta t = 1 \text{ s}$. It should be emphasised that using a different W_{\pm} does not significantly alter the conclusion derived subsequently.

It may be thought that one only needs to keep the noise due to the dark current below the quantum noise, that is $V_{\text{dark}} \leq V_{\text{x-noise}}$. However, such a requirement implies that the dark current can be as high as $\sim 10^6 \text{ A cm}^{-2}$ (point 1 in Fig. 10) which totally obliterates the dynamic range. V_{dark} against J_{dark} cuts the minimum likely exposure at point 2 in Fig. 10 where $J_{\text{dark}} = 1.3 \times 10^{-9} \text{ A cm}^{-2}$. A further increase in the dark current would shrink the dynamic range. Obviously point 2 where $V_{\text{dark}} = V_{\text{signal}}$ in Fig. 10 represent an upper limit for J_{dark} based on an ideal dynamic range constraint

$$J_{\text{dark}}A\Delta t \approx \frac{eAE_{\text{IR}}X_{\text{min}}}{W_{\pm}} \quad (14)$$

This requirement becomes even more rigid if one considers that the minimum signal in the radiation should be as high as the quantum noise which corresponds to point 3 in Fig. 10 where $V_{\text{dark}} = V_{\text{x-noise}}$. The corresponding dark current is an order of magnitude smaller. Another criterion would be that the noise due to J_{dark} should not exceed that due to the kTC noise in the detection system (allowing for some loss of dynamic range). From (12) and (13),

$$J_{\text{dark}} = \frac{C_{\text{px}}kT}{eA\Delta t} \quad (15)$$

which leads to a J_{dark} of $\sim 1 \times 10^{-9} \text{ A cm}^{-2}$; point 4 in Fig. 10. Table 3 lists the dark current requirements for a pixel of area $50 \times 50 \mu\text{m}^2$ based on $\Delta t = 1 \text{ s}$ and also shows the levels of dark current that have been typically reported for a-Se, PbI_2 , HgI_2 , PbO , CdZnTe photoconductors as examples.

For metal/a-Se/metal single-layer structures the dark current depends in a nonlinear fashion on the applied bias voltage and the metal/a-Se contacts. Because usable W_{\pm} values for acceptable sensitivity require high fields, which lead to high dark currents, it has been necessary to develop multilayer a-Se structures, as shown in Fig. 11 to reduce the dark current to an innocuous level. The n-layer is a very thin a-Se layer (a few microns) that has been appropriately doped to allow electron transport but trap holes (ideally $\tau_h = 0$ and $\tau_e = \infty$). The rate of emission of these deeply trapped holes in the n-layer is so small that there is no significant current injection into the bulk a-Se layer. Similarly, the p-layer is a thin a-Se that been appropriately doped to allow hole transport but trap electrons (ideally $\tau_h = \infty$ and $\tau_e = 0$). The rate of emission of deeply trapped holes is so small that the hole injection from the n-layer into a-Se is negligible. With these n- and p-layers, the fields at the metal electrodes are sufficiently small

Table 3: Dark current requirements based on dynamic range constraint and kTC noise considerations (Fig. 10) for direct-conversion detector for radiology

	Dynamic range constraint	kTC thermal noise limit	a-Se [9]	PbI_2 [3]	HgI_2 [4]	PbO [2]	CdZnTe [16]
J_{dark} (nA cm^{-2})	~ 1.3 (M) ~ 0.3 (C) ~ 6 (F)	~ 1.0 (M) ~ 0.07 (C) ~ 1 (F)	0.01 at $10 \text{ V } \mu\text{m}^{-1}$	1–5 at $0.5 \text{ V } \mu\text{m}^{-1}$	2–3 at $0.5 \text{ V } \mu\text{m}^{-1}$ with passivation	1 at $4 \text{ V } \mu\text{m}^{-1}$	1 at $4 \text{ V } \mu\text{m}^{-1}$

M = mammography, C = chest radiology, F = fluoroscopy. For each imaging mode, mean exposure and quantum noise specifications in [2] are used.

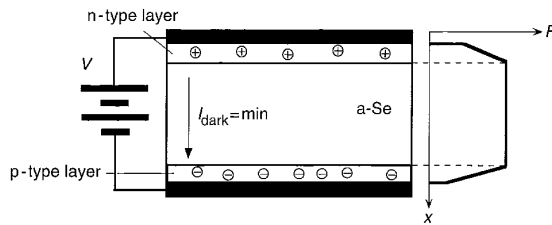


Fig. 11 Multilayer *p-i-n* type *a-Se* device structure for 'blocking' dark current

to prevent any substantial injection current from the electrodes. As indicated in Table 3, the dark current is $\sim 0.01 \text{ nA cm}^{-2}$ at a field of $10 \text{ V}/\mu\text{m}$, more than sufficient to satisfy the dark current requirements of flat-panel sensors.

In the case of PbI_2 photoconductors, there are two contradicting requirements. First is that the schubweg-limited charge collection efficiency can only be overcome by applying high fields, e.g. $F > 1 \text{ V}/\mu\text{m}$. The dark current however increases with the field and at these fields it is prohibitively high. There is therefore a compromise between the dark current and the schubweg limited sensitivity.

7 Medical and industrial applications

The medical applications for which flat-panel detectors are being developed and the new opportunities made possible with this technology are discussed in the context of the procedures currently used in clinical practice. All applications will benefit from the following general features of flat-panel detectors. (i) the compactness of the device permits use in situations where space is a premium such as operating room; (ii) the ability to be readout immediately after radiation exposure to verify patient positioning and appropriate image exposure speeds up the entire clinical examination; (iii) the ability to permit digital storage and communication within the hospital and beyond obviates problems with lost films and facilitates rapid diagnosis. (iv) the facilitation of computer-aided diagnosis and second opinions improve the accuracy of diagnosis; and, perhaps most importantly; (v) the possibility of improving image quality without increasing patient X-ray exposure due to the enhanced quantum efficiency of flat-panel detectors compared with conventional screen/film systems reduces radiation dose to patients and the associated risk. Next the requirements of specific important clinical imaging tasks and the improvements possible by digital X-ray imaging with flat-panel X-ray detectors are discussed.

7.1 Chest radiography

Radiography of the chest is technically difficult since diagnostic information is found in both very radiolucent (lung fields) and very radio-opaque (mediastinum) regions. This implies the need for a very high dynamic range detector. Previously it was found that by using very highly penetrating X-ray beams ($130\text{--}150 \text{ kVp}$), both these regions could be visualised simultaneously on a screen/film image despite the poor dynamic range of film. This is because the higher energy X-rays effectively reduce the contrast of the image and consequently reduce the dynamic range of the image to that of the film. This approach degrades the image quality in the lung fields to provide some information in the mediastinum.

Flat panel active matrix X-ray imagers have been configured for chest imaging and are commercially available. The foremost requirements are a very large field of

view, a reasonably high spatial resolution ($100\text{--}200 \mu\text{m}$ pixels) and a very large dynamic range to accommodate the different penetration of the lungs and mediastinum. Digital image processing can be used to equalise the appearance of the image and thus lower kVp will be used in the future so improving the image quality compared to screen/film systems.

7.2 Fluoroscopy

Fluoroscopy is the imaging systems in which X-ray motion pictures or video can be obtained. This technique is necessary in medicine when the functional operation of moving internal body parts (such as the moving stomach and gut) have to be visualised. Another application of fluoroscopy is in internal interventions controlled by X-ray imaging such as balloon angioplasty where a balloon is inflated within a blocked coronary artery to clear an obstruction. Here it is necessary to visualise the motion of the catheters with the arteries so as to move them to the disease site. Fluoroscopy is perhaps the most demanding potential application for flat-panel imaging systems. In fluoroscopic imaging the image must be updated at a very high rate (30 frames per second) to provide a believable appearance of motion. Very high patient doses often result from lengthy interventional fluoroscopic procedures. During these procedures, low radiation exposure rates must be used to reduce patient exposure to acceptable levels. This sets a stringent limit on the system performance since the image quality must still be adequate for visualisation of the surgical equipment and anatomy of interest. Therefore the imaging system must be X-ray quantum limited even at extremely low exposure levels. The current technology uses a large vacuum tube device called an X-ray image intensifier. Disadvantages of intensifiers include sensitivity to the earth's magnetic fields, extremely large bulk and distortions. Active matrix panels are more compact so permit better access to patients and since the panel is flat it is free from the geometrical distortions characteristic of X-ray image intensifiers. However, at the lowest exposure levels needed the irreducible noise from a large-area flat-panel array and its readout electronics is considerably larger than the quantum noise from the one or two X-rays per pixel per frame exposure level typical of fluoroscopy. This provides a main motivation for investigating photoconductors such as HgI_2 with increased X-ray sensitivity compared with *a-Se*. The increased gain promises to increase the signal to the point that fluoroscopic flat-panel systems could be quantum noise limited even at the lowest X-ray exposure levels. Alternative methods to effectively increase the X-ray sensitivity of *a-Se* are to incorporate an avalanche multiplication layer [28] or to use an amplifier integrated at each pixel [29].

7.3 Mammography

Mammography is the only projection X-ray imaging modality that attempts to visualise soft-tissue contrast and thus requires very poorly penetrating X-rays that are generated by using a low accelerating potential on the X-ray tube i.e. low kVp [30]. Film/screen is the current gold standard but it has a small dynamic range. Therefore extreme of breast compression to equalise the X-ray path length is needed so that the whole breast can be visualised. This breast compression is extremely uncomfortable and sometimes painful and is a major disincentive to patient acceptance. Digital mammography is still undergoing development but is becoming more important clinically [31]. Its advantages are increased dynamic range that potentially permits reduced breast compression, and the

ability to visualise radiographically dense breasts, which has a prevalence of 10–20% and in these cases acceptable images cannot be obtained with film/screen.

Another challenge is to make the pixels small enough to provide adequate resolution while maintaining at an acceptable cost. It is generally believed that while 100 μm pixels may not be quite small enough, 50 μm will be more than adequate. Both clinical and scientific studies are necessary to solve this resolution problem. The intrinsically high resolution of a-Se combined with the relative simplicity of the active matrix array design used for direct conversion and the possibility of using electrostatic focusing to ensure an essentially 100% effective fill-factor suggests that this approach is particularly applicable to mammography [32].

7.4 Industrial imaging

Low exposure is not a primary concern and therefore such applications are less demanding than medical imaging. X-ray imaging for cracks or macroscopic defects in various objects represents potential applications. Imaging of food, for example meat or fish to identify unwanted bones, are further possible applications. The current flat-panel detectors also have the potential for replacing X-ray film in crystal diffraction studies [33]. One can envisage various other applications in nondestructive testing.

8 Future

Flat-panel X-ray image detectors are still relatively new. Many advances in system design and improvements in system performance can be expected. These include: increased numbers of active elements per pixel, perhaps allowing an amplifier at every pixel as recently highlighted by Nathan [34], and integrated readout electronics to make an X-ray imager on glass; increased X-ray sensitivity either by use of improved photoconductors such as those discussed here with intrinsically lower W_{\pm} or by using a layer with avalanche gain. Indeed, according to Karim and Nathan [34], the overall signal gain can be substantially improved by incorporating an active element at each pixel.

The study of amorphous materials has been the scientific basis of the work described, but as forcefully pointed out by Mort [6] the theory to explain the behaviour of amorphous materials has lagged compared to their crystalline counterparts. Three amorphous materials are of importance for flat-panels. The first, discovered in antiquity, is optical glass; the second, discovered in the middle of the 19th century was the photoconductivity of selenium; and the last in the late 20th century is the dopable semiconductor, amorphous silicon. It is difficult to imagine flat-panel imagers without amorphous materials and the developments in materials science underlying the understanding and production of these materials will continue to be of great importance.

As fabrication techniques and device yields improve, more sophisticated switching structures with reduced coupling capacitance, lower leakage currents, smaller physical area and more robust operating characteristics will continue to be developed. These advances will improve the imaging performance of active matrix arrays until the dominant factor becomes the properties of the X-ray detection medium, even for the most demanding low signal level and high-resolution applications such as fluoroscopy and mammography.

The investigation of large-area flat-panel sensors presents a large variety of previously unexplored problems in detector physics. How they may be resolved has been discussed. However, direct-conversion flat-panel imagers using amorphous selenium are already permitting essentially

ideal X-ray imaging detectors to be constructed. The initial investment has been high but over time their image quality and labour-saving features will justify their cost. In the future, after the investment has been recouped, this approach has the potential due to its manufacturing simplicity to eventually be low cost. It is our opinion that flat-panel detectors are the unifying concept in X-ray medical imaging.

9 Acknowledgments

This work was supported by the National Cancer Institute of Canada (NCIC) through a Terry Fox Program project grant 'Imaging for cancer' and the Natural Sciences and Engineering Research Council of Canada through several grants. The authors also thank Anrad Corporation (Montreal), for additional support.

10 References

- 1 YAFFE, M.J., and ROWLANDS, J.A.: 'X-ray detectors for digital radiology', *Phys. Med. Biol.*, 1997, **42**, pp. 1–39
- 2 ROWLANDS, J.A., and YORKSTON, J.: in BEUTEL, J., KUNDEL, H.L. and VAN METTER, R.L. (Eds.) 'Handbook of medical imaging' (SPIE Press, Washington, 2000), Vol. 1, Chap. 4, (for the various flat-panel x-ray image sensors)
- 3 STREET, R.A., READY, S.E., RAHN, J.T., MULATO, M., SHAH, K., BENNETT, P.R., MEI, P., LU, J.-P., APTE, R.B., HO, J., VAN SCHUYLENBERGH, K., LEMMI, F., BOYCE, J.B., NYLEN, P., SCHIEBER, M., and HERMON, H.: 'High resolution, direct detection x-ray imagers', *Proc SPIE - Int. Soc. Opt. Eng.*, 2000, **3977**, pp. 418–428
- 4 SCHIEBER, M., HERMON, H., STREET, R.A., READY, S.E., ZUCK, A., VILENSKY, A., MELEKHOV, L., SHATUNOVSKY, R., MEERSON, E., and SAADO, Y.: 'Radiological x-ray response of polycrystalline mercuric iodide detectors', *Proc SPIE - Int. Soc. Opt. Eng.*, 2000, **3977**, pp. 48–55
- 5 KASAP, S.O.: in DIAMOND, A. (ed.): 'The handbook of imaging materials' (Marcel Dekker, New York, 1991), Chap. 8
- 6 MORT, J.: 'The anatomy of xerography-Its invention and evolution', (McFairland, London, UK, 1989)
- 7 KASAP, S.O., and ROWLANDS, J.A.: 'X-ray photoconductors and stabilized a-Se', *J. Mater. Sci. Mater. Electron.*, 2000, **11**, pp. 179–199
- 8 KNOLL, G.F.: 'Radiation detection and measurement', 3rd Edn. (Wiley, New York, 2000), Chap. 11
- 9 POLISCHUK, B., SHUKRI, Z., LEGROS, A., and ROUGEOT, H.: 'Selenium direct converter structure for static and dynamic x-ray detection in medical imaging', *Proc SPIE - Int. Soc. Opt. Eng.*, 1998, **3336**, pp. 494–504
- 10 HEIJNE, L., SCHAGEN, P., and BUINING, H.: 'An experimental photoconductive camera tube for television', *Philips Tech. Rev.*, 1954, **16**, p. 23
- 11 JACOBS, J., and BERGER, H.: 'Large-area photoconductive x-ray pickup-tube performance', *Electr. Eng.*, 1956, **75**, p. 158
- 12 BRAUERS, A., CONRADT, N., FRINGS, G., SCHIEBEL, U., POWELL, M.J., and GLASSE, C.: 'X-ray sensing properties of a lead oxide photoconductor combined with an amorphous silicon TFT array', *Mater. Res. Soc. Symp. Proc.*, 1998, **507**, pp. 321–326
- 13 WEISS, J.: 'Large-field cineradiography and image intensification utilising the TVX system', *Radiol.*, 1961, **76**, p. 264
- 14 SHAH, K.S., LUND, J.C., OLSCHNER, F., MOY, L., and SQUILLANTE, M.R.: 'Thallium bromide radiation detectors', *IEEE Trans. Nucl. Sci.*, 1989, **36**, p. 199
- 15 OUIMETTE, D.R., NUDELMAN, S., and AIKENS, R.: 'A new large area x-ray image sensor', *Proc. SPIE - Int. Soc. Opt. Eng.*, 1998, **3336**, pp. 470–476
- 16 ADACHI, S., HORI, N., SATO, K., TOKUDA, S., SATO, T., UEHARA, K., IZUMI, Y., NAGATA, H., YOSHIMURA, Y., and YAMADA, S.: 'Experimental evaluation of a-Se and CdTe flat-panel x-ray detectors for digital radiography and fluoroscopy', *Proc. SPIE - Int. Soc. Opt. Eng.*, 2000, **3977**, pp. 38–47
- 17 SQUILLANTE, M.R., ZHANG, J., ZHOU, C., BENNETT, P., and MOY, L.: 'New compound semiconductor materials for nuclear detectors', *Mater. Res. Soc. Symp. Proc.*, 1993, **302**, pp. 319–328
- 18 BENCIVELLI, W., BERTOLUCCI, E., BOTTIGLI, U., DEL GUERRA, A., MESSINEO, A., NELSON, W.R., RANDACCIO, P., ROSSO, V., ROSSO, P., and STEFANINI, A.: 'Evaluation of elemental and compound semiconductors for x-ray digital radiography', *Nucl. Instrum. Methods*, 1991, **A310**, pp. 210–214
- 19 WANG, Y., and HERRON, N.: 'X-ray photoconductive nanocomposites', *Science*, 1996, **273**, pp. 632–634
- 20 KASAP, S.O.: 'Optoelectronics and photonics: Principles and practices' (Prentice Hall, Upper Saddle River, 2001), Chap. 5
- 21 HECHT, K.: *Z. Phys.*, 1932, **77**, p. 235
- 22 KASAP, S.O.: 'X-ray sensitivity of photoconductors', *J. Phys. D, Appl. Phys.*, 2000, **33**, pp. 2853–2865

- 23 JUHASZ, C., VAEZI-NEJAD, S.M., and KASAP, S.O.: 'Drift mobility measurements on amorphous Se-based photoreceptors', *J. Imaging Sci.*, 1985, **29**, pp. 144–148
- 24 VAEZI-NEJAD, S.M., and JUHASZ, C.: 'Electrical properties of amorphous semiconductor selenium and its alloys I: monolayers', *Semicond. Sci. Technol.*, 1987, **2**, pp. 809–821
- 25 CHOQUETTE, M., ROUGEOT, H., MARTIN, J.-P., LAPERRIERE, L., SHUKRI, Z., and POLISCHUK, B.: 'Direct selenium x-ray detector for fluoroscopy, RF and radiography', *Proc. SPIE - Int. Soc. Opt. Eng.*, 2000, **3977**, pp. 128–136
- 26 STREET, R.A., RAHN, J.T., READY, S.E., SHAH, K., BENNET, P., DMITRIYEV, Y., MEI, P., LU, J.P., ABE, R.B., HO, K., VAN SCHUYLENBERGH, K., LEMMI, G., BOYCE, J.B., and NYLEN, P.: 'X-ray imaging using lead iodide as a semiconductor detector', *Proc. SPIE - Int. Soc. Opt. Eng.*, 1999, **3659**, pp. 36–46
- 27 TOKUDA, S., ADACHI, S., SATO, T., YOSHIMUTA, T., NAGATA, H., UEHARA, K., IZUMI, Y., TERANUMA, O., and YAMADA, S.: 'Experimental evaluation of a novel CdZnTe flat panel x-ray detector for digital radiography and fluoroscopy', *Proc. SPIE - Int. Soc. Opt. Eng.*, 2001, **4320**, pp. 140–147
- 28 HUNT, D.C., LUI, B., and ROWLANDS, J.A.: 'An experimentally validated theoretical model of avalanche multiplication x-ray noise in amorphous selenium', *Proc. SPIE - Int. Soc. Opt. Eng.*, 2000, **3977**, pp. 106–116
- 29 MATSUURA, N., ZHAO, W., HUANG, Z., and ROWLANDS, J.A.: 'Digital radiology using active matrix readout: amplified pixels for fluoroscopy', *Med. Phys.*, 1999, **26**, pp. 672–681
- 30 FAHRIG, R., ROWLANDS, R.A., and YAFFE, M.J.: 'X-ray imaging using amorphous selenium: optimal spectra for digital mammography', *Med. Phys.*, 1996, **23**, pp. 557–567
- 31 VENKATAKRISHNAN, V., YAVUZ, M., NIKLASON, L.T., OPSAHL-ONG, B., HAN, S., LANDBERG, C., NEVIN, R., HAMBERG, L., and KOPANS, D.B.: 'Experimental and theoretical spectral optimization for digital mammography', *Proc. SPIE - Int. Soc. Opt. Eng.*, 1999, **3659**, pp. 142–149
- 32 ZHAO, W., ROWLANDS, J.A., GERMANN, S., WAECHTER, D.F., and HUANG, Z.: 'Digital radiology using self-scanned readout of amorphous selenium: design considerations for mammography', *Proc. SPIE - Int. Soc. Opt. Eng.*, 1995, **2432**, pp. 250–259
- 33 LEE, D.L., RODRICKS, B., HOFFBERG, M.G., WILLIAMS, C.L., GOLDEN, K.P., and JEROMIN, L.S.: 'Filtered-gain calibration and its effect on frequency-dependent DQE and image quality in Se-based general radiography and full-field mammographic digital imaging', *Proc. SPIE - Int. Soc. Opt. Eng.*, 2001, **4320**, pp. 121–126
- 34 KARIM, K., and NATHAN, A.: 'Alternate pixel architectures for large area medical imaging', *Proc. SPIE - Int. Soc. Opt. Eng.*, 2001, **4320**, pp. 35–46